Please cite this article in press as: Colloc'h et al., Mapping Hydrophobic Tunnels and Cavities in Neuroglobin with Noble Gas under Pressure, Biophysical Journal (2017), https://doi.org/10.1016/j.bpj.2017.10.014

Biophysical *Journal*
Article

Biophysical Society

# Mapping Hydrophobic Tunnels and Cavities in Neuroglobin with Noble Gas under Pressure

Nathalie Colloc'h,[1,*] Philippe Carpentier,[2,3] Laura C. Montemiglio,[4] Beatrice Vallone,[4] and Thierry Prangé[5]
[1]ISTCT CNRS UNICAEN CEA Normandie University, CERVOxy Team, Centre Cyceron, Caen, France; [2]CEA/DRF/BIG/CBM/BioCat LCBM CNRS UMR 5249, Université Grenoble Alpes, Grenoble, France; [3]European Synchrotron Radiation Facility, Grenoble, France; [4]Instituto Pasteur–Fondazione Cenci Bolognetti and Dipartimento di Scienze Biochimiche "A. Rossi Fanelli", Sapienza Università di Roma, Roma, Italy; and [5]LCRB, UMR 8015 CNRS Université Paris Descartes, Paris, France

ABSTRACT Internal cavities are crucial for conformational flexibility of proteins and can be mapped through noble gas diffusion and docking. Here we investigate the hydrophobic cavities and tunnel network in neuroglobin (Ngb), a hexacoordinated heme protein likely to be involved in neuroprotection, using crystallography under noble gas pressure, mostly at room temperature. In murine Ngb, a large internal cavity is involved in the heme sliding mechanism to achieve binding of gaseous ligands through coordination to the heme iron. In this study, we report that noble gases are hosted by two major sites within the internal cavity. We propose that these cavities could store oxygen and allow its relay in the heme proximity, which could correspond to NO location in the nitrite-reductase function of Ngb. Thanks to a recently designed pressurization cell using krypton at high pressure, a new gas binding site has been characterized that reveals an alternate pathway for gaseous ligands. A new gas binding site on the proximal side of the heme has also been characterized, using xenon pressure on a Ngb mutant (V140W) that binds CO with a similar rate and affinity to the wild-type, despite a reshaping of the internal cavity. Moreover, this study, to our knowledge, provides new insights into the determinants of the heme sliding mechanism, suggesting that the shift at the beginning of helix G precedes and drives this process.

## INTRODUCTION

Cavities present within proteins are crucial for conformational flexibility, playing a role in dynamics and in functional mechanisms. Defects in the protein core introduce instabilities that facilitate conformational changes and sampling of the different conformational substates that lead to catalysis or to regulation of activity (1,2). Moreover, routes for substrate and product to and from the active site can be mapped by the identification of cavities and tunnels within the protein matrix (3–5).

Noble gas labeling with xenon or krypton constitutes a versatile tool for the determination of hydrophobic cavities and tunnels that can be accessed by diffusion or become available by protein structure fluctuations (6–8). Consequently, xenon has often been used to probe pathways and binding sites for dioxygen or for other ligands (9,10). Noble gases interact with proteins through noncovalent weak-energy London forces, their binding constant depending on their polarizability. Thus, gas occupancy in a given hydrophobic binding site may be ranked as follows: argon $<$ krypton $<$ xenon (11,12). Raising the pressure can be exploited to increase the gas occupancy up to saturation following a pressure-response curve, and to expand the volume of the gas binding sites (13–15).

Globins are prototypical systems in which the internal cavity network has been extensively investigated because it plays a key role in controlling ligand migration and protein function, as assessed directly with ligands trapped after photodissociation and indirectly through labeling with xenon (16–19). In neuroglobin (Ngb), a neuronal hexacoordinated globin likely involved in neuroprotection (20,21), an unusually large and dynamic network of cavities has been detected (22–24). As shown in murine Ngb, the heme slides inside a large internal cavity upon gaseous ligand binding to the heme iron, following the hexa- to pentacoordination mechanism (25,26).

Several direct and indirect pieces of evidence indicate that Ngb plays a role in the protection of neurons from hypoxia, reducing the damage due to NO and reactive oxygen species and preventing apoptosis (27,28). Moreover, Ngb is upregulated in mammals that are chronically exposed to hypoxic environment such as moles or mammals that are capable of

*Submitted June 12, 2017, and accepted for publication October 6, 2017.*
*Correspondence: colloch@cyceron.fr
Editor: Elizabeth Rhoades.
https://doi.org/10.1016/j.bpj.2017.10.014

Please cite this article in press as: Colloc'h et al., Mapping Hydrophobic Tunnels and Cavities in Neuroglobin with Noble Gas under Pressure, Biophysical Journal (2017), https://doi.org/10.1016/j.bpj.2017.10.014



prolonged underwater dives (29–31). Intriguingly, Ngb overexpression has been proposed as a mechanism for tumor cells to survive in oxygen deprivation. Therefore, depending on pathological conditions, Ngb appears to be a protein that can rescue or promote pathological states. However, the precise biochemical mechanisms through which Ngb is involved in the above multifaceted role are still unclear. Nevertheless, direct NO and nitrate scavenging and cytochrome *c* reduction have been characterized in vitro, and could account directly or indirectly for most of the effects observed upon hypoxic or radical stress (32,33).

To shed light on how the structural features of Ngb could account for reactivity toward gaseous ligands that are markedly different from those observed and characterized in detail on hemoglobin and myoglobin, it is therefore of interest to characterize the dynamics and chemical nature of the internal matrix. The high conservation throughout evolution of the Ngb sequence in vertebrates indicates that only a limited variability is allowed, suggesting a strong purifying selection and thus tight functional constraints (34).

As indicated by the crystal structures of unliganded and CO-bound Ngb, the internal heme cavity plays a key role in the ligand binding mode through its structural flexibility and plasticity. The cavity network in Ngb has already been analyzed using Xe labeling (13,24). To investigate further the gaseous ligand diffusion pathway within the internal heme cavity and possible subtle differences in the chemical nature of the complex cavity system in Ngb, we determined the structures of the wild-type Ngb (WT-Ngb) under argon and krypton pressure (from 10 to 50 bar) at room temperature, and compared them to the previously determined Ngb structures under Xe pressure (13). Moreover, thanks to a recently designed pressurization cell based on the soak-and-freeze methodology, krypton can be used at a much higher pressure, allowing us to populate new gas binding sites that can suggest novel diffusion pathways for oxygen (35,36). We then determined Ngb structure at 100 K under 100 bar of Kr. Finally, we investigated the reshaping and plasticity of the heme cavity by determining and analyzing the structure of a mutant V140W (V140W-Ngb) under pressurized Xe (10, 20, and 30 bar). Although the cavity in this mutant is smaller than in WT-Ngb, it binds CO with similar rates and affinities (37).

## METHODS

WT-Ngb and V140W-Ngb production, purification, and crystallization have been described previously (37). Crystals of WT-Ngb and V140W-Ngb were obtained by the hanging drop technique at 293 K, using a 1:1 mixture of protein (10 mg $mL^{-1}$) and reservoir solution (1.6 M ammonium sulfate, 0.1 M MES pH 6.5, 10%(v/v) dioxane). In all cases, this led to crystals in the rhombohedral space group R32 with one monomer per asymmetric unit. Molecules of dioxane have also sometimes been localized in the electron density map.

Data collections under pressurized gas at room temperature (RT) were recorded using the pressurization cell previously described (38), for which a crystal mounted in a quartz capillary fitted to the cell is pressurized and maintained under gas pressure during the data collection. Data collections were recorded both gas-less and under Ar or Kr pressure (10, 20, 30, 40, and 50 bar) for WT-Ngb and under Xe pressure (10, 20, and 30 bar) for V140W-Ngb. In the case of Xe, special care was taken to orient crystals, with respect to the beam, to limit traveling of diffraction spots in the gas atmosphere as described in (38).

A data collection for WT-Ngb with a 100-bar pressure of Kr has been recorded with the recently designed cryogenic cell based on the soak-and-freeze methodology (36). A crystal, cryo-protected with the mother liquor reservoir solution and glycerol 25% v/v, is inserted in a tube, which is filled with 100 bar Kr and pressurized during a few minutes of soaking. The sample is flash-frozen when the crystal is released to drop it into the cold dense fluid phase of Kr and falls to the bottom of the tube immersed in a liquid nitrogen bath. The gas pressure is then released, allowing recovery of the frozen crystal in the liquid nitrogen bath. Data collections are then performed at 100 K.

Diffraction data were collected at the European Synchrotron Radiation Facility in Grenoble, France at the beamline BM30A for WT-Ngb with an ADSC Q315r CCD detector and at the beamline BM16 for V140W-Ngb with an ADSC Q210r CCD detector. Exposure times were 3–4 s per frame for an oscillation angle of 1°. Data were indexed and integrated by MOSFLM (39) or by XDS (40), then scaled and merged by SCALA, and intensities were converted in structure-factor amplitudes using TRUNCATE (all from the CCP4 package (41)).

The structure of the Protein Data Bank (PDB) entry 1Q1F, in which heteroatoms and alternate side-chain positions were removed, was used as a starting model for rigid body refinement. Once the model was positioned, refinement steps were performed with restrained geometric parameters (coordinates and thermal factors) using REFMAC (42). The graphic program COOT (43) was used to visualize $|2Fobs - Fcalc|$ and $|Fobs - Fcalc|$ electron density maps and for manual rebuilding during refinement steps. All RT diffraction data were collected at a wavelength of 0.980 Å far from the Xe K-edge (0.3587 Å). However, the $f''$ anomalous contribution to the scattering factors for Xe (3.1 electrons) and Kr (0.6 electrons) at this wavelength were sufficiently high to unambiguously identify the presence of these atoms from peaks in anomalous difference maps. The 100 K data collection was collected at 0.8556 Å, then optimized for the Kr K-edge (0.8655 Å). Ar atoms were assessed using information for gas sites in the internal cavity, normally void of electron density in the reference structure of Ngb. Determination of gas occupancies were deduced from model-independent anomalous maps for each Kr and Xe pressure measurement by using the iron anomalous signal as an internal reference. They were also deduced for each gas pressure measurement from peaks height values corresponding to the gas in OMIT maps at the beginning of the refinements. They were fixed during refinement steps with unrestrained thermal factors. The resulting gas B-factors were similar for a given binding site regardless of the applied gas pressure. Tables S5, S6, and S7 summarize data collection and refinement statistics for WT-Ngb under Ar or Kr pressure, and V140W-Ngb under Xe pressure, respectively.

Cavity volumes were calculated using the program CASTp (44) with a probe radius of 1.4 Å, considering the heme atoms as part of the protein. Tunnels were computed using CAVER (45) on WT-Ngb or V140W-Ngb native structures using a probe radius of 0.9 Å and a starting point corresponding to the storage site. Figs. 1, 3, and 4 and Fig. S1 have been prepared using the software PYMOL (DeLano Scientific, Palo Alto, CA).

## RESULTS

### WT-type Ngb structures under the pressure of xenon

Xenon binding sites in Ngb have already been described at 100 K under a pressure of 20 bar (24) and at RT under pressures of 10, 20, and 30 bar (13). Interestingly, the two

Please cite this article in press as: Colloc'h et al., Mapping Hydrophobic Tunnels and Cavities in Neuroglobin with Noble Gas under Pressure, Biophysical Journal (2017), https://doi.org/10.1016/j.bpj.2017.10.014



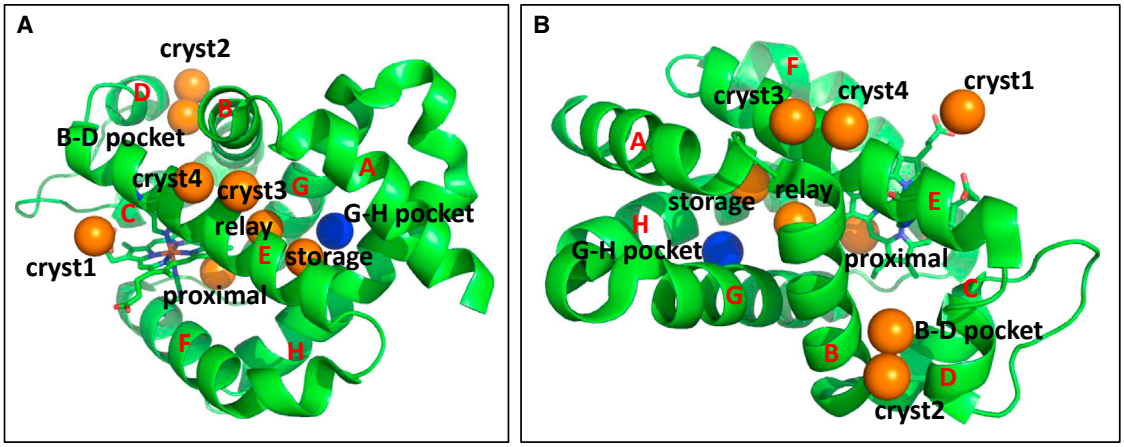


FIGURE 1 (*A* and *B*) Neuroglobin in two different orientations in cartoon representation, with the heme, the distal histidine, and the proximal histidine shown in stick representation; the xenon and krypton atoms are shown in orange and blue spheres, respectively.

main Xe binding sites are located within the large internal heme cavity, which is empty of any ordered water molecules in the native structure. These two major sites termed "NGB-III" and "NGB-IV" in (13) and "XeIII" and "XeIV" in (24) were proposed to define gaseous ligand pathways on their way to and from the heme, respectively. They will be termed here the "storage" and "relay" sites, with the relay site located between the storage site and the heme. Xe binds also in a solvent-accessible surface pocket between helices B and D, where water molecules are loosely bound; this site was termed "NGB-II" in (13) and "XeII" in (24) and will be termed here the "B-D pocket". Four Xe binding sites, located at crystallographic interfaces, will be termed "cryst1" to "cryst4" (they were termed "NGB-I", "NGB-V", "NGB-VI", and "NGB-VII" in (13) and note that "cryst1" was also termed "XeI" in (24)). They are mostly packing-dependent pockets not involved in any functional process, and will not be further discussed here. The different xenon binding sites are shown in Fig. 1.

## WT-type Ngb structures under the pressure of krypton and argon

Crystallographic structures under pressurized Kr show that krypton binds to Ngb within the storage and relay sites and the B-D pocket but no Kr atom was observed in the cryst1–cryst4 sites up to 100 bar of pressure. Occupancies increase with pressure up to 80% in the B-D pocket, up to 100% in the storage site and up to 35% in the relay site (Fig. 2; Fig. S1, *A* and *B*; Table S1). Crystallographic structures under pressurized Ar show that argon binds to Ngb only within the storage site at 40 and 50 bar pressure with occupancies up to 30% (Fig. 2; Table S2).

At 100 bar, Kr binds with a 20% occupancy in a new surface pocket between helices G and H (which will be termed here the "G-H pocket"), which is very close to the back of the internal cavity (Fig. 1, and 4 *A*; Fig. S1 *C*; Table S1). The G-H pocket is empty in the native structure, but a water molecule was positioned in the structures under Xe or Kr pressure at 30 bar and above, revealing that a gas molecule was likely to be present but with too low an occupancy to be considered as such. In the anomalous maps, the peaks were also too low to be significant.

## Ngb mutant V140W under the pressure of xenon

The mutation of $Val^{140}$ to Trp induces only slight structural modifications, as already described when comparing the two deoxy structures at 100 K (PDB: 4NZI for the V140W-Ngb and PDB: 1Q1F for WT-Ngb) (37). The V140W-Ngb native structure at RT here described shows only minor differences with the PDB: 4NZI structure (100 K) with a root-mean-square deviation on the C$\alpha$ chain of 0.24 Å. The comparison between the WT-Ngb and V140W-Ngb structures at RT reveals a slight displacement toward the bulk of the H helix where the mutation is located (root-mean-square deviation $>$ 0.5 Å on the C$\alpha$ chain for residues 135–140) with no change in the CD and EF loops. However, the main structural modification between the two structures corresponds to the large reduction of the volume of the internal heme cavity of 24% as expected (from 225 to 172 $Å^3$), because the mutation was designed for this purpose by introducing a bulkier side chain.

Xenon binds to V140W-Ngb within all Xe sites already described for the WT-Ngb (13). Also, occupancies for Xe in the different pockets (B-D pocket, cryst1–cryst4 sites) are quite similar in the WT and in the mutant (Table S3). We expected the storage and relay sites occupancies to be lower in V140W-Ngb, considering that the volume of the internal cavity has been reduced by 24% with respect to WT-Ngb. However, the opposite trend was found: Xe binds with significant higher occupancies in the storage site, and especially in the relay site within the mutant compared to

Please cite this article in press as: Colloc'h et al., Mapping Hydrophobic Tunnels and Cavities in Neuroglobin with Noble Gas under Pressure, Biophysical Journal (2017), https://doi.org/10.1016/j.bpj.2017.10.014



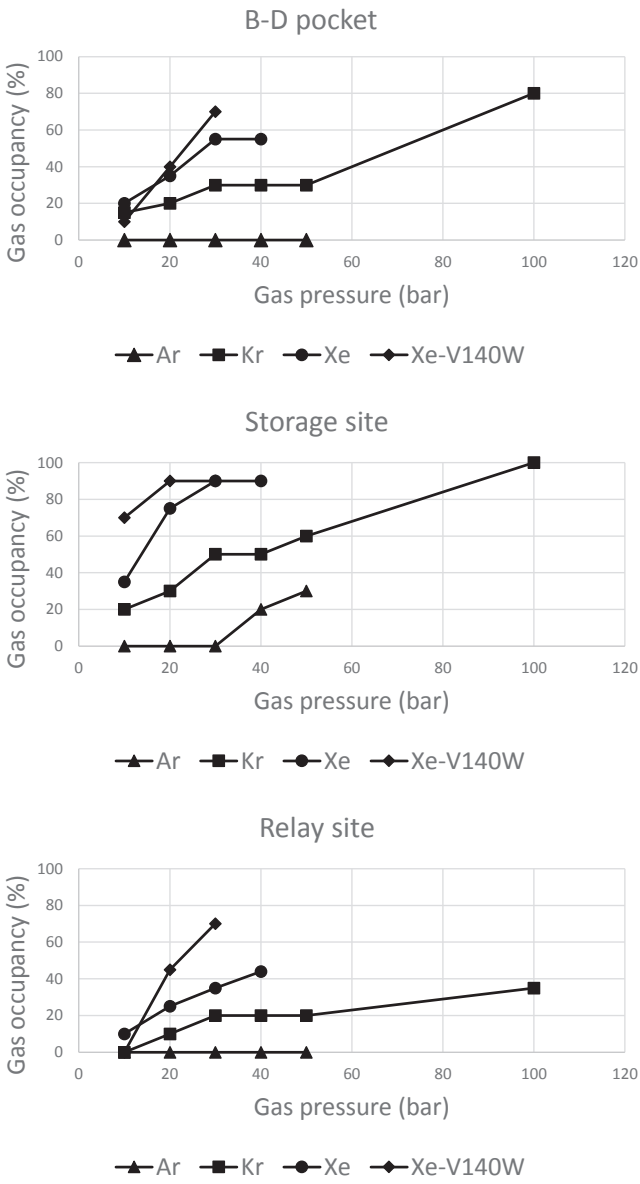


FIGURE 2 Gas occupancy as a function of pressure within the B-D pocket, the storage, and the relay sites for Ar (*triangle*), Kr (*square*), and Xe in WT-Ngb (*circle*) and for Xe in V140W-Ngb (*diamond*).

the WT (Fig. 2; Table S3). This can be explained by the fact that gas occupancies arise from a subtle combination of the binding sites' hydrophobicity and volumes on the one hand, and the number and strength of the induced-dipole-dipole interactions on the other (13,46). Indeed, in our case, the higher occupancies detected in the mutant result from a higher affinity and adaptation of the hydrophobic cavity—the volume of which is smaller but better suited to the specific radius of the gas than shown in the WT-Ngb.

Interestingly, in V140W-Ngb, Xe at 30 bar pressure binds to a new site on the proximal side of the heme, which will be termed the "proximal" site, with a 60% occupancy. Mechanistically, the Xe atom binds into the location of Phe$^{106}$ side chain, which is displaced away from the heme (Fig. 3; Fig. S1 *D*). The shift of Phe$^{106}$ induces a series of structural modifications at the beginning of helix G (residues Arg$^{102}$–Ser$^{107}$) with a shift of almost 1 Å of the C$\alpha$ chain toward the bulk and, notably, a large displacement of Leu$^{103}$. In V140W-Ngb at 20 bar Xe, the presence of the Xe atom is identified in the anomalous map at the position of Phe$^{106}$ side chain, but not clearly in the electron density map. Moreover, it is worth mentioning that a weak anomalous peak for this gas within the Phe$^{106}$ side-chain position is already identifiable in WT-Ngb at 30 and 40 bar Xe, and in WT-Ngb at 100 bar Kr.

## Analysis of cavity volumes

Comparison of cavity volumes can only be done between RT protein structures, because at 100 K, the volume of the unit cell is compressed by almost 4%, inducing a de facto reduction of the volume of the protein, and hence a shrinkage of volume of all pockets and cavities. Surface pocket volumes are less sensitive to the presence of a bound gas than internal cavity, and their expansion is limited (data not shown). In WT-Ngb, the storage and relay sites are both located in the large internal heme cavity, which has a volume 224 Å$^3$. The volume of this cavity expands with the applied gas pressure (Fig. S2). Cavity volume expansion reaches 60% with Xe, 40% with Kr, and 20% with Ar. Interestingly, in the case of argon, the volume of the cavity expands even when no gas is visible in the electron density map, as seen in Ngb under 10, 20, and 30 bar pressure, indicating that argon is present in the cavity but not structurally ordered.

In V140W-Ngb, the heme cavity of volume 172 Å$^3$ also expands with the applied Xe pressure (Fig. S2). Expansion

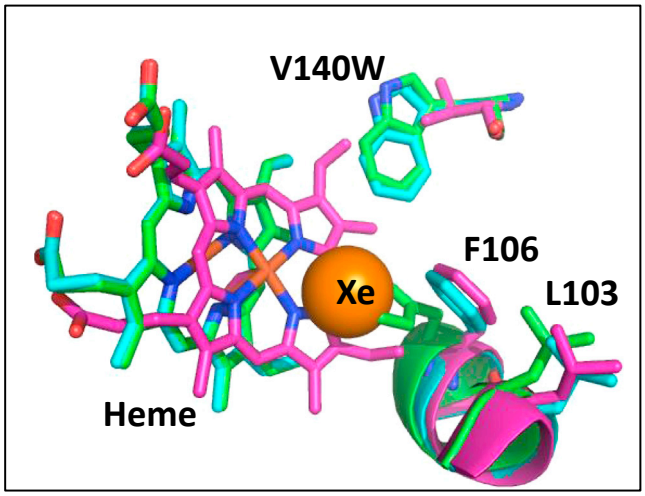


FIGURE 3 Neuroglobin proximal side with L103, F106, V140, or W140 residues and the heme shown in stick representation, the Xe atom as an orange sphere, and the beginning of the G helix in cartoon representation in V140W-Ngb (*green*), V140W-Ngb-Xe-30 (*cyan*), and CO-Ngb (PDB: 1W92, *pink*).

Please cite this article in press as: Colloc'h et al., Mapping Hydrophobic Tunnels and Cavities in Neuroglobin with Noble Gas under Pressure, Biophysical Journal (2017), https://doi.org/10.1016/j.bpj.2017.10.014



reaches 50% expansion at 20 bar, but it is lower at 30 bar (34%) due to the remodeling of the cavity (shift of Phe$^{106}$).

### Analysis of tunnels

Analysis of tunnels computed by CAVER (45) in WT-Ngb shows that the main tunnel connects the storage site directly to the bulk (Fig. 4 *B*, *blue*), flanked by the residue Tyr$^{88}$ (as already described (24,27)). However, a secondary tunnel is also detected, connecting the new Kr binding site in the G-H pocket to the protein surface (Fig. 4 *B*, green).

Analysis of tunnels in V140W-Ngb compared to WT-Ngb shows that two main tunnel volumes are in reverse order in size (Fig. 4, *B* and *C*). The mutation of Val$^{140}$ by a Trp induces a reduction of the tunnel connecting the storage site to the bulk, and therefore the tunnel that goes through the G-H pocket (secondary in WT; in *green* Fig. 4 *B*, *green*) becomes, in that case, the main pathway to the bulk (Fig. 4 *C*, *blue*).

## DISCUSSION

The use of noble gas pressurized crystallography is a way to characterize hydrophobic tunnels and cavities that are likely to be relevant binding sites for gaseous ligands such as $O_2$, CO, or NO (18,24,27). Argon possesses a number of electrons similar to the dioxygen molecule and was postulated to produce a kind of oxygen synergy, allowing it to adapt to hypoxic conditions (47), suggesting that Ar could mimic $O_2$. In Ngb, Ar binds only in the storage site, suggesting that this site corresponds to the $O_2$ storage site as previously suggested (24). This site would then be at the lowest energy level. Similarly, Kr and Xe possess van der Waals radii similar to that of $O_2$, allowing it to map the dioxygen pathway in Ngb on its way to and from the heme through the relay and storage sites (24,27).

In the relay site, Kr and Xe are lined by five hydrophobic residues (Val$^{68}$, Ile$^{72}$, Val$^{109}$, Leu$^{113}$, and Tyr$^{137}$). These five residues were previously described using coarse-grained simulations and high pressure crystallography as constituting the mechanical nucleus around which Ngb hinges upon ligand binding during its conformational transition (48,49). The key role of Val$^{68}$ and Val$^{109}$ in controlling ligand migration has been assessed by mutation studies (50,51). In CO-Ngb, Xe still binds to the relay and storage sites, but with slightly decreased occupancies (24). The mechanical nucleus is thus not affected by the heme sliding mechanism, being rigidified by pressure (49). In contrast, the main channel connecting the storage site to the bulk is closed by pressure, thus decreasing CO migration (49,52).

The G-H pocket in which Kr binds at 100 bar is located in a surface pocket close to the storage site. In cytoglobin, another hexacoordinated globin, Xe binds at a site corresponding to the Ngb storage site and also at a site located deeper in the heme cavity (16), corresponding in Ngb to a position halfway between the storage site and the G-H pocket. The G-H pocket could then mark out a novel pathway for the gaseous ligand in Ngb from the bulk toward the heme, tracing an alternate route that would span the G-H pocket and the storage and relay sites (Fig. 4).

The neuroprotective properties of Ngb could be mediated, among other mechanisms, through NO scavenging activity when acting as nitrite reductase (27,51). The reaction of NO with the heme-Fe-bound $O_2$ yielding to nitrate as the final product, is very rapid. Our data support the hypothesis that the Xe location in the relay site, after the heme has slid upon oxygen binding, could correspond to the physiological NO location before reaction with Fe-$O_2$ (24,32). Therefore, the relay site could act as a reservoir for NO, and thus contributes to the efficiency of the scavenging process. We identified an alternative mode of access to this site—i.e., via the G-H pocket. And in a nitrite oxide binding domain, crystallography under pressurized xenon also allowed us to identify alternative routes for the gas-ligand diffusion (53).

The mutant V140W provides, to our knowledge, new insight into the determinants of the heme sliding mechanism

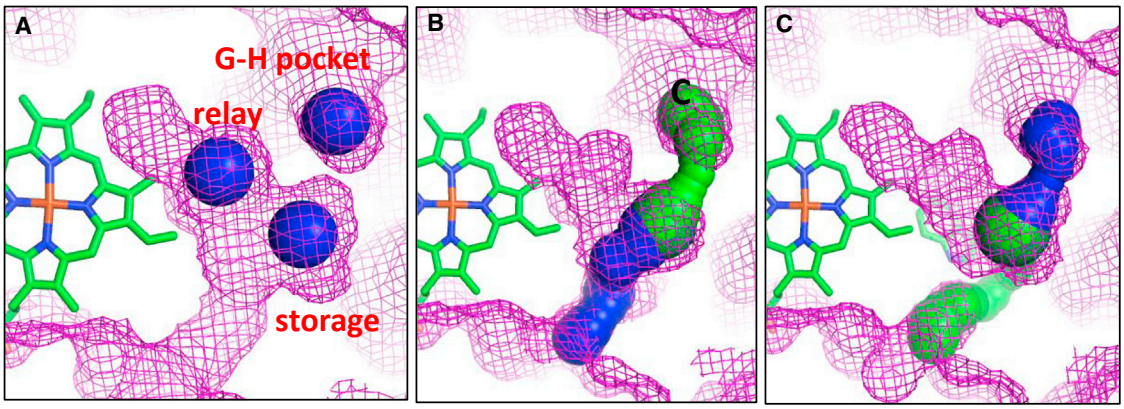


FIGURE 4 Surface of Ngb (in *mesh*, considering the heme atoms as part of the protein) with the heme shown in stick representation. (*A*) Given here is the WT-Ngb with the Kr atoms (*blue sphere*) in the storage and relay sites and in the new binding site within the G-H pocket. WT-Ngb (*B*) and V140W-Ngb (*C*) with the main tunnel in blue and the secondary one in green were computed by CAVER.

Please cite this article in press as: Colloc'h et al., Mapping Hydrophobic Tunnels and Cavities in Neuroglobin with Noble Gas under Pressure, Biophysical Journal (2017), https://doi.org/10.1016/j.bpj.2017.10.014



upon ligand binding. This mutant shows unaffected CO affinity as compared to the WT (37). In this mutant, Xe at 30 bar binds to a new proximal site, at the location of the $Phe_{106}$ side chain (Fig. 3). $Phe^{106}$ is the residue most affected by the heme sliding mechanism (26). Superposition of the V140W-Ngb-Xe-30 structure with the CO-Ngb structure (PDB: 1W92) shows that Xe in the proximal site would clearly collide with the heme in the CO-Ngb structure (Fig. 3, in *pink*). The Xe atom induces the displacement of the $Phe^{106}$ side chain in the position observed in the CO-Ngb structure, i.e., when the heme has slid. In turn, the side chain of $Phe^{106}$ displaces the side chain of $Leu^{103}$ to the position it occupies in the CO-Ngb structure (Fig. 3, in *pink*). Therefore, the structural modifications around the heme are clearly similar in CO-Ngb and in V140W-Ngb-Xe-30 structures. Xe at 30 bar pressure mimics the effect of heme sliding on the $Phe^{106}$ side chain, which is pushed away from the heme.

These structural modifications parallel the ones observed in the Ngb V101F mutant, another substitutions that introduces additional bulk in the heme proximal side (37). Indeed $Phe^{101}$ was observed to affect the $Phe^{106}$ and $Leu^{103}$ positions similarly to Xe bound at its proximal site (49). Also the shift of the beginning of helix G (residues $Arg^{102}$–$Ser^{107}$) occurs in V140W-Ngb-Xe-30 and V101F structures in the absence of heme sliding. These findings led us to conclude that the area surrounding $Phe^{106}$ seems to be structurally prepared to move upon gaseous ligand binding. The concerted displacement of $Phe^{106}$, $Leu^{103}$, and of the helical segment 102–107 can therefore occur in the absence of heme sliding and possibly precedes and drives it.

Inert rare gases are interesting probes/agents for investigating biological systems. They have been mainly studied for their medical interest (54). Xenon is a remarkably safe inhalational clinical anesthetic, and has shown very promising neuroprotective properties with almost no side effects (55–57). Argon has also been described to have neuroprotective properties (58,59), whereas krypton seems a less promising therapeutic agent because of side effects (60). The Meyer-Overton rule describes the high correlation between anesthetic potency and their solubility in lipids. Scales that assess the in vivo potency of inhaled anesthetics are based on the minimum-alveolar anesthetic concentration (MAC) immobility that is associated with well-defined behavioral endpoints (61). Xe, which has the highest solubility in lipids and the highest polarizability due to its high number of electrons, also has the highest anesthetic potency (i.e., the lowest MAC immobility) compared to Kr and Ar. In turn, Kr, which has a higher solubility in lipids and a higher polarizability than Ar, would also have a higher anesthetic potency (Table S4) (12,62,63).

Analysis of the few proteins whose structures were determined under pressure of Xe, Kr, and Ar showed that gas occupancies can indeed reproduce gas polarizabilities and solubilities (11,12). In Ngb, occupancies of Xe are always higher than occupancies of Kr, themselves higher than occupancies of Ar at an equivalent pressure for the same binding site (Fig. 2). Ratio of Xe to Kr occupancies range between 1.75 and 2.5, in the same order as their ratio of polarizabilities and solubilities (1.6 and 2.7, respectively). Ratio of Kr to Ar occupancies in the storage site range between 2 and 2.5, in the same order as their ratio of polarizabilities and solubilities (1.5 and 3, respectively). The ratio of their anesthetic potencies (i.e., ratio of their MAC immobility in rat, 4.5 and 3.7 for Kr/Xe and Ar/Kr, respectively) is also quite similar to their ratio of occupancies.

Gas occupancy in a given binding site rises with the applied gas pressure (Fig. 2) and the internal heme cavity volume rises with the applied gas pressure (Fig. S2). The relationship between the expansion of volume of the internal cavity and the gas occupancy in the storage and relay sites is linear with $R^2 = 0.8742$, 0.9813, and 0.9291 for Kr and Xe in WT-Ngb, and Xe in V140W-Ngb, respectively (Fig. S3) (calculation performed without V140W-Ngb-Xe-30, because the volume of the heme cavity is modified by the shift of the $Phe^{106}$ side chain). No relationship was found between Ar occupancy and internal cavity volume, likely due to Ar-induced volume expansion even when no gas was visible in the electron density map. It has been hypothesized that the occupancy of internal cavities by anesthetics, including gaseous ones, leads to protein stabilization, reducing the motion that underlies normal protein activity. Gas occupancy or volume expansion has, for example, been related to gas-induced inhibition of activity for urate oxidase and for elastase (11,15). Occupancy and/or volume expansion of cavities would shift the population of conformational substates toward those that enhance or inhibit protein activity (64–66). This process could thus underlie neuroprotection and anesthesia mechanisms. It is therefore relevant to analyze rigorously the interaction of noble gases with the protein matrix and to correlate their binding with protein features and dynamics that are likely to govern function, to provide a base for understanding the mechanism of their anesthetic effect.

## Data availability

The atomic coordinates and structure factors have been deposited in the Protein Data Bank: WT-Ngb under 50 bar Ar (PDB: 5NVI); WT-Ngb under 50 bar and 100 bar krypton (PDB: 5NW6 and 5O17, respectively); and V140W-Ngb gasless and under 20 and 30 bar xenon (PDB: 5O18, 5O1K, and 5O27, respectively).

## SUPPORTING MATERIAL

Three figures and seven tables are available at http://www.biophysj.org/biophysj/supplemental/S0006-3495(17)31129-3.

Please cite this article in press as: Colloc'h et al., Mapping Hydrophobic Tunnels and Cavities in Neuroglobin with Noble Gas under Pressure, Biophysical Journal (2017), https://doi.org/10.1016/j.bpj.2017.10.014



## AUTHOR CONTRIBUTIONS

N.C., B.V., and T.P. conceived the project. L.C.M. and B.V. expressed, purified, and crystallized WT-Ngb and mutant. N.C., P.C., and T.P. contributed to the experiment. N.C. and T.P. analyzed the data. N.C., P.C., B.V., and T.P. wrote the manuscript.

## ACKNOWLEDGMENTS

The authors thank Giovanna Avella (Sapienza Università di Roma) for mutant V140W-Ngb production, purification, and crystallization. They also thank Peter van der Linden for fruitful discussions and essential technical support, the staff members of beamline BM16, Jean-Luc Ferrer, Michel Pirrochi, and the staff members of beamline BM30A, at the European Synchrotron Radiation Facility (ESRF, Grenoble, France) for their technical help and assistance. N.C. thanks Jacques H. Abraini (Université de Caen, France) for fruitful discussions and Buz Barstow for comments and corrections.

## REFERENCES

1. Hubbard, S. J., K. H. Gross, and P. Argos. 1994. Intramolecular cavities in globular proteins. *Protein Eng.* 7:613–626.
2. Lee, C., J. S. Maeng, …, M. H. Yu. 2001. Cavities of $\alpha_1$-antitrypsin that play structural and functional roles. *Protein Sci.* 10:1446–1453.
3. López, C. J., Z. Yang, …, W. L. Hubbell. 2013. Conformational selection and adaptation to ligand binding in T4 lysozyme cavity mutants. *Proc. Natl. Acad. Sci. USA.* 110:E4306–E4315.
4. Morrison, C. N., J. A. Hoy, …, D. C. Rees. 2015. Substrate pathways in the nitrogenase MoFe protein by experimental identification of small molecule binding sites. *Biochemistry.* 54:2052–2060.
5. Kitahara, R., Y. Yoshimura, …, F. A. A. Mulder. 2016. Detecting $O_2$ binding sites in protein cavities. *Sci. Rep.* 6:20534.
6. Knapp, J. E., R. Pahl, …, W. E. Royer, Jr. 2009. Ligand migration and cavities within Scapharca Dimeric HbI: studies by time-resolved crystallography, Xe binding, and computational analysis. *Structure.* 17:1494–1504.
7. Prangé, T., M. Schiltz, …, R. Fourme. 1998. Exploring hydrophobic sites in proteins with xenon or krypton. *Proteins.* 30:61–73.
8. Tilton, R. F., Jr., I. D. Kuntz, Jr., and G. A. Petsko. 1984. Cavities in proteins: structure of a metmyoglobin-xenon complex solved to 1.9 Å. *Biochemistry.* 23:2849–2857.
9. Hiromoto, T., S. Fujiwara, …, H. Yamaguchi. 2006. Crystal structure of 3-hydroxybenzoate hydroxylase from *Comamonas testosteroni* has a large tunnel for substrate and oxygen access to the active site. *J. Mol. Biol.* 364:878–896.
10. Wade, R. C., P. J. Winn, …, Sudarko. 2004. A survey of active site access channels in cytochromes P450. *J. Inorg. Biochem.* 98:1175–1182.
11. Colloc'h, N., G. Marassio, and T. Prangé. 2010. Protein-noble gas interactions investigated by crystallography on three enzymes. Implication on anesthesia and neuroprotection mechanisms. *In* Current Trends in X-Ray Crystallography. A. Chandrasekaran, ed. InTech, Rijeka, Croatia, pp. 285–308.
12. Quillin, M. L., W. A. Breyer, …, B. W. Matthews. 2000. Size versus polarizability in protein-ligand interactions: binding of noble gases within engineered cavities in phage T4 lysozyme. *J. Mol. Biol.* 302:955–977.
13. Abraini, J. H., G. Marassio, …, N. Colloc'h. 2014. Crystallographic studies with xenon and nitrous oxide provide evidence for protein-dependent processes in the mechanisms of general anesthesia. *Anesthesiology.* 121:1018–1027.
14. Colloc'h, N., J. Sopkova-de Oliveira Santos, …, J. H. Abraini. 2007. Protein crystallography under xenon and nitrous oxide pressure: comparison with in vivo pharmacology studies and implications for the mechanism of inhaled anesthetic action. *Biophys. J.* 92:217–224.
15. Marassio, G., T. Prangé, …, N. Colloc'h. 2011. Pressure-response analysis of anesthetic gases xenon and nitrous oxide on urate oxidase: a crystallographic study. *FASEB J.* 25:2266–2275.
16. de Sanctis, D., S. Dewilde, …, M. Bolognesi. 2004. Mapping protein matrix cavities in human cytoglobin through Xe atom binding. *Biochem. Biophys. Res. Commun.* 316:1217–1221.
17. Savino, C., A. E. Miele, …, B. Vallone. 2009. Pattern of cavities in globins: the case of human hemoglobin. *Biopolymers.* 91:1097–1107.
18. Brunori, M., and Q. H. Gibson. 2001. Cavities and packing defects in the structural dynamics of myoglobin. *EMBO Rep.* 2:674–679.
19. Schlichting, I., and K. Chu. 2000. Trapping intermediates in the crystal: ligand binding to myoglobin. *Curr. Opin. Struct. Biol.* 10:744–752.
20. Burmester, T., B. Weich, …, T. Hankeln. 2000. A vertebrate globin expressed in the brain. *Nature.* 407:520–523.
21. Burmester, T., and T. Hankeln. 2009. What is the function of neuroglobin? *J. Exp. Biol.* 212:1423–1428.
22. Abbruzzetti, S., S. Faggiano, …, C. Viappiani. 2009. Ligand migration through the internal hydrophobic cavities in human neuroglobin. *Proc. Natl. Acad. Sci. USA.* 106:18984–18989.
23. Bocahut, A., S. Bernad, …, S. Sacquin-Mora. 2009. Relating the diffusion of small ligands in human neuroglobin to its structural and mechanical properties. *J. Phys. Chem. B.* 113:16257–16267.
24. Moschetti, T., U. Mueller, …, B. Vallone. 2009. The structure of neuroglobin at high Xe and Kr pressure reveals partial conservation of globin internal cavities. *Biophys. J.* 97:1700–1708.
25. Vallone, B., K. Nienhaus, …, G. U. Nienhaus. 2004. The structure of murine neuroglobin: novel pathways for ligand migration and binding. *Proteins.* 56:85–92.
26. Vallone, B., K. Nienhaus, …, G. U. Nienhaus. 2004. The structure of carbonmonoxy neuroglobin reveals a heme-sliding mechanism for control of ligand affinity. *Proc. Natl. Acad. Sci. USA.* 101:17351–17356.
27. Ascenzi, P., A. di Masi, …, M. Marino. 2016. Neuroglobin: from structure to function in health and disease. *Mol. Aspects Med.* 52:1–48.
28. Baez, E., V. Echeverria, …, G. E. Barreto. 2016. Protection by neuroglobin expression in brain pathologies. *Front. Neurol.* 7:146.
29. Mitz, S. A., S. Reuss, …, T. Burmester. 2009. When the brain goes diving: glial oxidative metabolism may confer hypoxia tolerance to the seal brain. *Neuroscience.* 163:552–560.
30. Williams, T. M., M. Zavanelli, …, D. S. Kliger. 2008. Running, swimming and diving modifies neuroprotecting globins in the mammalian brain. *Proc. Biol. Sci.* 275:751–758.
31. Avivi, A., F. Gerlach, …, T. Hankeln. 2010. Neuroglobin, cytoglobin, and myoglobin contribute to hypoxia adaptation of the subterranean mole rat Spalax. *Proc. Natl. Acad. Sci. USA.* 107:21570–21575.
32. Brunori, M., A. Giuffrè, …, B. Vallone. 2005. Neuroglobin, nitric oxide, and oxygen: functional pathways and conformational changes. *Proc. Natl. Acad. Sci. USA.* 102:8483–8488.
33. Fago, A., A. J. Mathews, …, T. Brittain. 2006. The reaction of neuroglobin with potential redox protein partners cytochrome $b_5$ and cytochrome *c*. *FEBS Lett.* 580:4884–4888.
34. Roesner, A., C. Fuchs, …, T. Burmester. 2005. A globin gene of ancient evolutionary origin in lower vertebrates: evidence for two distinct globin families in animals. *Mol. Biol. Evol.* 22:12–20.
35. Kalms, J., A. Schmidt, …, P. Scheerer. 2016. Krypton derivatization of an $O_2$-tolerant membrane-bound [NiFe] hydrogenase reveals a hydrophobic tunnel network for gas transport. *Angew. Chem. Int. Ed. Engl.* 55:5586–5590.
36. Lafumat, B., C. Mueller-Dieckmann, …, P. Carpentier. 2016. Gas-sensitive biological crystals processed in pressurized oxygen and krypton atmospheres: deciphering gas channels in proteins using a novel 'soak-and-freeze' methodology. *J. Appl. Cryst.* 49:1478–1487.

Please cite this article in press as: Colloc'h et al., Mapping Hydrophobic Tunnels and Cavities in Neuroglobin with Noble Gas under Pressure, Biophysical Journal (2017), https://doi.org/10.1016/j.bpj.2017.10.014




37. Avella, G., C. Ardiccioni, …, B. Vallone. 2014. Engineering the internal cavity of neuroglobin demonstrates the role of the haem-sliding mechanism. *Acta Crystallogr. D Biol. Crystallogr.* 70:1640–1648.

38. Schiltz, M., T. Prangé, and R. Fourme. 1994. On the preparation and x-ray data collection of isomorphous xenon derivatives. *J. Appl. Cryst.* 27:950–960.

39. Leslie, A. G. 2006. The integration of macromolecular diffraction data. *Acta Crystallogr. D Biol. Crystallogr.* 62:48–57.

40. Kabsch, W. 2010. XDS. *Acta Crystallogr. D Biol. Crystallogr.* 66:125–132.

41. Collaborative Computational Project, Number 4. 1994. The CCP4 suite: programs for protein crystallography. *Acta Crystallogr. D Biol. Crystallogr.* 50:760–763.

42. Murshudov, G. N., A. A. Vagin, and E. J. Dodson. 1997. Refinement of macromolecular structures by the maximum-likelihood method. *Acta Crystallogr. D Biol. Crystallogr.* 53:240–255.

43. Emsley, P., and K. Cowtan. 2004. Coot: model-building tools for molecular graphics. *Acta Crystallogr. D Biol. Crystallogr.* 60:2126–2132.

44. Binkowski, T. A., S. Naghibzadeh, and J. Liang. 2003. CASTp: computed atlas of surface topography of proteins. *Nucleic Acids Res.* 31:3352–3355.

45. Chovancova, E., A. Pavelka, …, J. Damborsky. 2012. CAVER 3.0: a tool for the analysis of transport pathways in dynamic protein structures. *PLOS Comput. Biol.* 8:e1002708.

46. Schiltz, M., R. Fourme, and T. Prangé. 2003. Use of noble gases xenon and krypton as heavy atoms in protein structure determination. *Methods Enzymol.* 374:83–119.

47. David, H. N., B. Haelewyn, …, J. H. Abraini. 2012. Ex vivo and in vivo neuroprotection induced by argon when given after an excitotoxic or ischemic insult. *PLoS One.* 7:e30934.

48. Bocahut, A., S. Bernad, …, S. Sacquin-Mora. 2011. Frontier residues lining globin internal cavities present specific mechanical properties. *J. Am. Chem. Soc.* 133:8753–8761.

49. Colloc'h, N., S. Sacquin-Mora, …, E. Girard. 2017. Determinants of neuroglobin plasticity highlighted by joint coarse-grained simulations and high pressure crystallography. *Sci. Rep.* 7:1858.

50. Astudillo, L., S. Bernad, …, J. Miksovska. 2012. Conformational dynamics in human neuroglobin: effect of $His^{64}$, $Val^{68}$, and $Cys^{120}$ on ligand migration. *Biochemistry.* 51:9984–9994.

51. Tejero, J., C. E. Sparacino-Watkins, …, M. T. Gladwin. 2015. Exploring the mechanisms of the reductase activity of neuroglobin by site-directed mutagenesis of the heme distal pocket. *Biochemistry.* 54:722–733.

52. Hamdane, D., L. Kiger, …, M. C. Marden. 2005. High pressure enhances hexacoordination in neuroglobin and other globins. *J. Biol. Chem.* 280:36809–36814.

53. Winter, M. B., M. A. Herzik, Jr., …, M. A. Marletta. 2011. Tunnels modulate ligand flux in a heme nitric oxide/oxygen binding (H-NOX) domain. *Proc. Natl. Acad. Sci. USA.* 108:E881–E889.

54. Dickinson, R., and N. P. Franks. 2010. Bench-to-bedside review: molecular pharmacology and clinical use of inert gases in anesthesia and neuroprotection. *Crit. Care.* 14:229.

55. David, H. N., B. Haelewyn, …, J. H. Abraini. 2008. Neuroprotective effects of xenon: a therapeutic window of opportunity in rats subjected to transient cerebral ischemia. *FASEB J.* 22:1275–1286.

56. Lavaur, J., M. Lemaire, …, P. P. Michel. 2016. Neuroprotective and neurorestorative potential of xenon. *Cell Death Dis.* 7:e2182.

57. Maze, M. 2016. Preclinical neuroprotective actions of xenon and possible implications for human therapeutics: a narrative review. *Can. J. Anaesth.* 63:212–226.

58. Sanders, R. D., D. Ma, and M. Maze. 2010. Argon neuroprotection. *Crit. Care.* 14:117.

59. Ulbrich, F., and U. Goebel. 2016. The molecular pathway of argon-mediated neuroprotection. *Int. J. Mol. Sci.* 17:E1816.

60. Jawad, N., M. Rizvi, …, D. Ma. 2009. Neuroprotection (and lack of neuroprotection) afforded by a series of noble gases in an in vitro model of neuronal injury. *Neurosci. Lett.* 460:232–236.

61. Campagna, J. A., K. W. Miller, and S. A. Forman. 2003. Mechanisms of actions of inhaled anesthetics. *N. Engl. J. Med.* 348:2110–2124.

62. Koblin, D. D., Z. Fang, …, J. R. Trudell. 1998. Minimum alveolar concentrations of noble gases, nitrogen, and sulfur hexafluoride in rats: helium and neon as nonimmobilizers (nonanesthetics). *Anesth. Analg.* 87:419–424.

63. Růzicka, J., J. Benes, …, V. Markvartová. 2007. Biological effects of noble gases. *Physiol. Res.* 56 (*Suppl 1*):S39–S44.

64. Eckenhoff, R. G. 2001. Promiscuous ligands and attractive cavities: how do the inhaled anesthetics work? *Mol. Interv.* 1:258–268.

65. Johansson, J. S., H. Zou, and J. W. Tanner. 1999. Bound volatile general anesthetics alter both local protein dynamics and global protein stability. *Anesthesiology.* 90:235–245.

66. Vemparala, S., C. Domene, and M. L. Klein. 2010. Computational studies on the interactions of inhalational anesthetics with proteins. *Acc. Chem. Res.* 43:103–110.